INTERNATIONAL JOURNAL FOR NUMERICAL METHODS IN FLUIDS
Int. J. Numer. Meth. Fluids 2002; **38**:227–253 (DOI: 10.1002/fld.214)

On the influence of numerical schemes and subgrid–stress models on large eddy simulation of turbulent flow past a square cylinder

A. Nakayama*,† and S. N. Vengadesan

Division of Global Development Science, Graduate School of Science and Technology, Kobe University, Kobe 657-8501, Japan

SUMMARY

Influence of finite difference schemes and subgrid-stress models on the large eddy simulation calculation of turbulent flow around a bluff body of square cylinder at a laboratory Reynolds number, has been examined. It is found that the type and the order of accuracy of finite-difference schemes and the subgrid-stress model for satisfactory results are dependent on each other, and the grid resolution and the Reynolds number. Using computational grids manageable by workstation-level computers, with which the near-wall region of the separating boundary layer cannot be resolved, central-difference schemes of realistic orders of accuracy, either fully conservative or non-conservative, suffer stability problems. The upwind-biased schemes of third order and the Smagorinsky eddy-viscosity subgrid model can give reasonable results resolving much of the energy-containing turbulent eddies in the boundary layers and in the wake and representing the subgrid stresses in most parts of the flow. Noticeable improvements can be obtained by either using higher order difference schemes, increasing the grid resolution and/or by implementing a dynamic subgrid stress model, but each at a cost of increased computational time. For further improvements, the very small-scale eddies near the upstream corners and in the laminar sublayers need to be resolved but would require a substantially larger number of grid points that are out of the range of easily accessible computers. Copyright © 2002 John Wiley & Sons, Ltd.

KEY WORDS: large eddy simulation; square cylinder; finite difference schemes; subgrid-stress models

1. INTRODUCTION

As the cost of large-scale numerical computations is decreasing continually, heavier computational loads are tolerated more in practical calculations of turbulent flows. The large eddy simulation (LES) technique that was been thought to be too expensive for practical calculations now has a high potential to be exploited in various engineering applications if accuracy and applicabilities are assured. There has been extensive work in making this

*Correspondence to: A. Nakayama, Division of Global Development Science, Graduate School of Science and Technology, Kobe University, Kobe 657-8501, Japan.
† E-mail: nakayama@kobe-u.ac.jp

Received November 1999
Revised April 2001

technique a useful tool, but no single procedure has yet emerged as a standard [1–4]. Particularly, the state of development of LES applied to bluff bodies as summarized by the outcome of the Rottach–Egern workshop [5] is disappointingly inconclusive. It remarks that 'no single simulation was uniformly good' and that 'the effect proved very difficult to analyze is the choice of numerical method'. While use of the difference schemes and subgrid-stress models did vary among the participants at the workshop, it should also be noted that none used the same number of grid points and resolution. Important questions such as what differencing scheme is suitable, which subgrid model is more accurate and how the near wall region should be represented with what boundary condition, are not answered in a definite way.

The schemes evaluated at the workshop [5], included second-order central difference schemes as well as third-order upwind differencing methods. Caution is given to the use of the upwind differencing due to its numerical dissipation, but central difference schemes are not endorsed either, due to their inherent unstable nature. Recently, higher order conservative schemes are proposed by Morinishi *et al.* [6] as methods that are free of dissipative penalty and stability problems, but their necessity and adequacy have not been demonstrated in the bluff body LES of relatively large Reynolds number.

As to the subgrid-stress models, inadequacies of the widely used Smagorinsky eddy viscosity model have been amply stressed by many reviews [1–4]. Many newer models such as the one-equation model (Yoshizawa and Horiuti [7]), dynamic model of eddy-viscosity type (Germano *et al.* [8]), scale-similarity-type models (Bardina *et al.* [9]), mixed dynamic models (e.g. Vreman *et al.* [10]) are proposed and improvements of varying degree have been demonstrated, but the standard Smagorinsky model is still widely used with apparent success. An even more recent investigation by Fureby *et al.* [11] reports that LES results are virtually independent of the details of the subgrid model provided the cutoff wave number is within the inertial subrange. Sohankar *et al.* [12] show results with various models but the differences are of the same order or smaller than the effects of changing the grid resolution or considering the blockage effects in the test flow. Furthermore, Bouris and Bergeles [13] points out that resolving the very fine-scale motion near-wall is more important than the choice of models and they used a two-dimensional grid as large as 300×350 to place the first point from the wall at a very short distance of 10^{-4} of the cylinder side, but at a cost of giving away representing the three-dimensional motion, and they report marked improvements. Many claims of improved accuracy are based on comparisons set up by each developer and are not always on the same grounds. The models, for example, are often evaluated by a calculation of simple wall flow of very low Reynolds number with grid resolution exceeding the viscous scale or close (e.g. Horiuti [14] and Najjar and Tafti [15]). All of these results need to be carefully interpreted in extending to the bluff body LES of high Reynolds number.

As pointed out by the workshop review [5], 'the most useful were those cases in which a single group did more than one calculation', which was done by only two groups. In the present work, though not all factors may be addressed at the same time, we take the two most important elements of the LES and make a comparative study. For this purpose, we examine different difference schemes and the typical subgrid models keeping other conditions identical and evaluate again what the suitable type and order of difference scheme is, and the subgrid model for bluff body LES of a typical engineering scale with a realistic grid resolution. We do this for the now standard benchmark test case of Lyn's [16, 17] square cylinder flow at

the Reynolds number of 22 000. Accuracies and behavior of numerical schemes and their coding are first evaluated at lower Reynolds numbers. Once again, emphasis is placed on the engineering scales with affordable computer resources that do not allow the first grid point from the cylinder surface to be anything closer than the order of tens of the wall units. This implies the importance of how the near-wall flow is represented. Since there is no alternative at this time to the nonslip or the wall-law, or perhaps log-power (Werner and Wengle [18]) boundary conditions as a sure method, we evaluate all other aspects of the methods on a rather specific assumption of nonslip condition with Van Driest-type damping if a point happens to fall in its effective range, which occurs only and surely near the reattachment points.

2. BASIC EQUATIONS

We consider the flow past a square cylinder placed in an otherwise uniform flow of U_{in} in the x_1 direction, with its axis placed along the x_3 direction and its center of the downstream surface at the origin of the rectangular coordinate system (x_1, x_2, x_3) (Figure 1). If the filtered velocity component in x_i direction is $\langle u_i \rangle$ and the filtered pressure is $\langle p \rangle$, the filtered equations

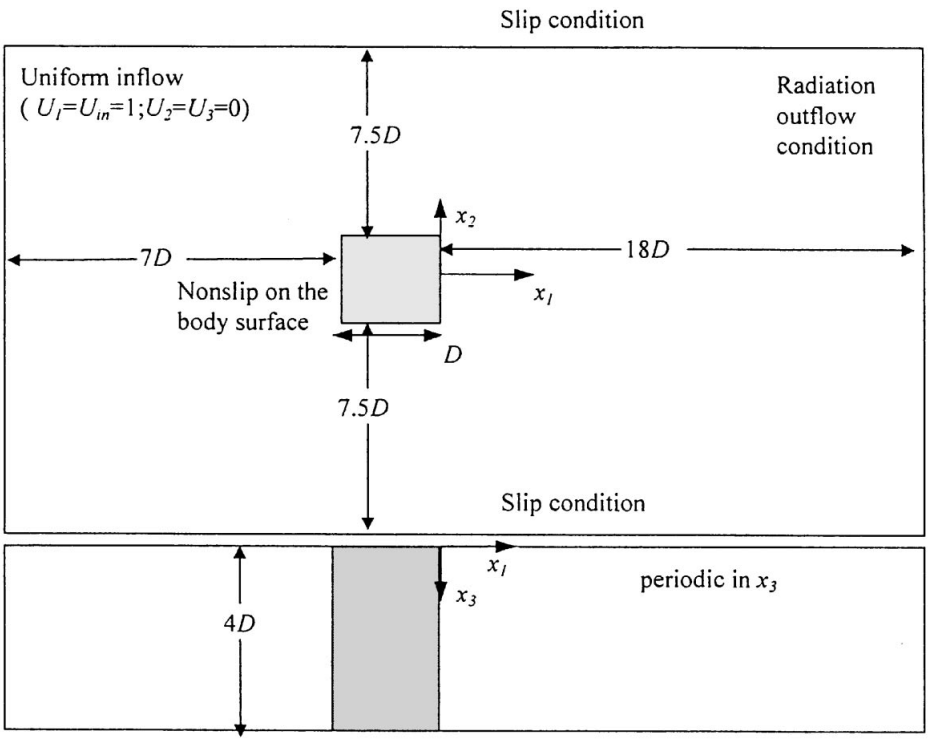

Figure 1. Computational domain and boundary conditions.

of motion are

$$\frac{\partial\langle u_i\rangle}{\partial t}+\frac{\partial\langle u_i\rangle\langle u_j\rangle}{\partial x_j}=-\frac{1}{\rho}\frac{\partial\langle p\rangle}{\partial x_i}+\nu\frac{\partial^2\langle u_i\rangle}{\partial x_j\partial x_j}+\frac{\partial\tau_{ij}}{\partial x_j}$$
$$\frac{\partial\langle u_i\rangle}{\partial x_i}=0 \tag{1}$$

where ρ and ν are the fluid density and the kinematic viscosity, respectively, $\tau_{ij}=-\langle u_iu_j\rangle+\langle u_i\rangle\langle u_j\rangle$ is the subgrid turbulence stress, and $\langle\,\rangle$ indicates spatial filtering.

The eddy viscosity model for the subgrid stress is

$$\tau_{ij}=-\frac{2}{3}k_S\delta_{ij}+2\nu_GS_{ij} \tag{2}$$

where S_{ij} is the rate of strain tensor of the filtered velocity, ν_G is the subgrid eddy-viscosity coefficient and k_S is the subgrid turbulence kinetic energy. For ν_G and k_S, we use the Smagorinsky model

$$\nu_G=2(C_S\Delta)^2\sqrt{S_{ij}S_{ij}},\quad k_S=\frac{\nu_G^2}{(C_k\Delta)^2} \tag{3}$$

Here C_S and C_k are the constants for which we use the numerical values 0.13 and 0.094, respectively and Δ is the grid size and is taken to be the geometric average of the grid spacing in three directions, $(\Delta x_1\Delta x_2\Delta x_3)^{1/3}$.

We will also use the dynamic procedure to determine the value of C_S due to Germano *et al.* [8] with Lilly's modification [19], in which the coefficient C_S is determined from

$$C_S^2=-\frac{[\Lambda_{ij}M_{ij}]}{2[M_{ij}M_{ij}]} \tag{4}$$

where

$$\Lambda_{ij}=\langle u_iu_j\rangle-\langle u_i\rangle\langle u_j\rangle$$
$$M_{ij}=\hat{\Delta}^2|\hat{S}_{ij}|\hat{S}_{ij}-\Delta^2|S_{ij}|S_{ij} \tag{5}$$

and [ ] represents averaging in the spanwise direction, $\hat{\ }$ represents test filtering with filter width $\hat{\Delta}=\alpha\Delta$. The explicit test filtering for quantity f, for example, is done by a discrete form of

$$\langle\hat{f}\rangle=\langle f\rangle+\frac{\hat{\Delta}^2}{24}\left(\frac{\partial^2\langle f\rangle}{\partial x_1^2}+\frac{\partial^2\langle f\rangle}{\partial x_2^2}+\frac{\partial^2\langle f\rangle}{\partial x_3^2}\right) \tag{6}$$

which represents a Gaussian filtering. We chose $\alpha=2$ and, as has been done by Lilly [19], when the right-hand side of Equation (4) becomes negative, C_S is set to zero.

The boundary conditions are shown in Figure 1 and are: the nonslip condition on the cylinder surface; slip condition on the top and bottom boundaries; the periodic boundary conditions in the spanwise direction; the uniform inflow condition along the upstream boundary; and radiation outflow at the downstream boundary. These are the standard boundary conditions recommended to the participants of the workshop [5].

Table I. Computational grids.

Key	Grid size	Minimum grid width	Points inside cylinder
G1	$101 \times 91 \times 21$	0.05	21×21
G2	$130 \times 111 \times 21$	0.04	26×29

Table II. Differencing schemes for convective terms.

Key	Description
CD2	Conventional 2nd-order central difference
CC2	Conservative 2nd-order central difference
CD4	Conventional 4th-order central difference
UB3	3rd-order upwind-biased difference
UB5	5th-order upwind-biased difference

3. NUMERICAL METHODS

3.1. Calculation domain and computational grid

Calculated flow configuration and the coordinate definition are given in Figure 1. The calculation domain chosen here is larger upstream of the cylinder than specified for the participants of the workshop [5] but the rest are about the same. We have chosen two grid systems to be used for all computations as shown in Table I. Points in both grids are uniformly distributed over the cylinder surface and in the spanwise direction. The spacing in the streamwise and cross-stream directions are stretched, gradually going away from the cylinder. The first grid is $101 \times 91 \times 21$ which can be managed fairly easily even on personal computers. This will be referred to as grid G1. Grid G2 is $130 \times 111 \times 21$ which is about 50 per cent larger in terms of the total number points, but still can be managed by most workstation computers, and the smallest spacing on the surface is 0.04 times the cylinder side D.

3.2. Discretization of convective terms

The convective terms are discretized by five different methods, namely, conventional non-conservative central differencing schemes of 2nd- and 4th-order accuracy, the upwind-biased schemes of 3rd- and 5th-order accuracy and the fully conservative 2nd-order central differencing scheme of Morinishi [6]. These will be referred to as CD2, CD4, UB3, UB5 and CC2, respectively as summarized in Table II. The conventional differencing schemes of different orders are generated by a single general formula given by Fornberg [20]. The 3rd-order one coincides with the UTOPIA scheme. The fully conservative scheme follows Morinishi's [6] formula. Then, these are written in explicit Adams–Bashforth form with respect to time.

The rest of the numerical methods are fixed for all cases. The viscous and the subgrid terms are differenced by the 2nd-order central difference, and written in fully implicit form so that time advancing is done using an SOR iterative method. The pressure is solved using the HSMAC procedure. These procedures are the same as those used and verified in Nakayama and Noda [21].

4. VALIDATION AT LOW REYNOLDS NUMBER

For the purpose of validating the computer codes and examining the relative accuracies and stability of different schemes, calculations are first performed at low Reynolds numbers. The Reynolds number, Re, we refer to is defined by the upstream uniform flow velocity U_{in} and the cylinder side D. For test cases at very low Reynolds numbers of 50 and 100, only coarse grid G1 is used for all cases except for the case of $Re = 100$, the scheme CD4 for which calculation on grid G1 diverged if started from the uniform initial flow condition, and the results with grid G2 are shown.

First, Figure 2(a) and (b) show the results for $Re = 50$, represented by the plots of contours of constant vorticity and streamlines. At this low Reynolds number, the flow is steady and symmetric with twin vortices in the separation bubble. All the results agree very well confirming the basic calculation procedure. Slight differences in the shapes of the streamlines are due mainly to the method of tracing the streamlines, which sensitively depends on how the stream function is computed from the calculated velocity vectors.

Figure 3(a) and (b) show similar results for the case of $Re = 100$. At this Reynolds number, the flow starts to be unsteady and the results shown here are all at nondimensional time $tU_{in}/D = 20$ from the initial uniform flow condition. The results of low-order central difference scheme CD2 on G1 do not show unsteadiness and the 4th-order non-conservative scheme CD4 diverged if run on grid G1. The 3rd-order upwind biased scheme UB3 and CD4 on fine grid G2 agree very well. In order to confirm that these results are correct, the values of some computed parameters are summarized in Table III comparing with the results of Franke *et al.* [22]. Additional calculation was also made at $Re = 150$ using UB3 on grid G1, so that closer comparison with the calculation of Franke *et al.* [22] can be made. The results are shown in Figure 4 for two phases of the vortex shedding cycle and good agreement is confirmed.

Figure 5(a) and (b) show the results for $Re = 200$ for various schemes for the two grids. According to Sohankar *et al.* [23], the flow starts to show three dimensionality and secondary vortices at this Reynolds number. CD2 scheme on G1 shows the pressure oscillation upstream of the cylinder. The same scheme on the fine grid G2 does not show this instability but appears to give only steady flow. UB3 on G1 does not show vortex shedding either, while the conservative scheme CC2 on G1 shows a weak shedding. The results of UB3 and CD4 on grid G2 agree well with each other and the results of Sohankar *et al.* [23] obtained for the same condition. These three methods were further run for higher Reynolds number of 500, in which the vortex shedding becomes very strong and transition to turbulent flow begins, and it is thought that an LES method for turbulent flows would have to be able to cope with this type of flow. The non-conservative scheme CD4, however, diverged at an early stage of calculation but UB3 and CC2 schemes produced results that are shown in Figure 6(a) and (b). The CC2 scheme on grid G1 starts to show instability like that seen with the non-conservative central difference schemes at a lower Reynolds number of 200. UB3 and CC2 schemes on grid G2 gave results at this and higher Reynolds numbers, though their accuracies cannot be assured at the present time.

The results of these laminar flow calculations may be summarized as below. While the magnitudes and the nature of errors associated with various finite difference schemes vary depending on the type and the order of accuracy of the schemes and the grid resolution, they all increase in magnitude with increasing Reynolds number. With the present fineness or

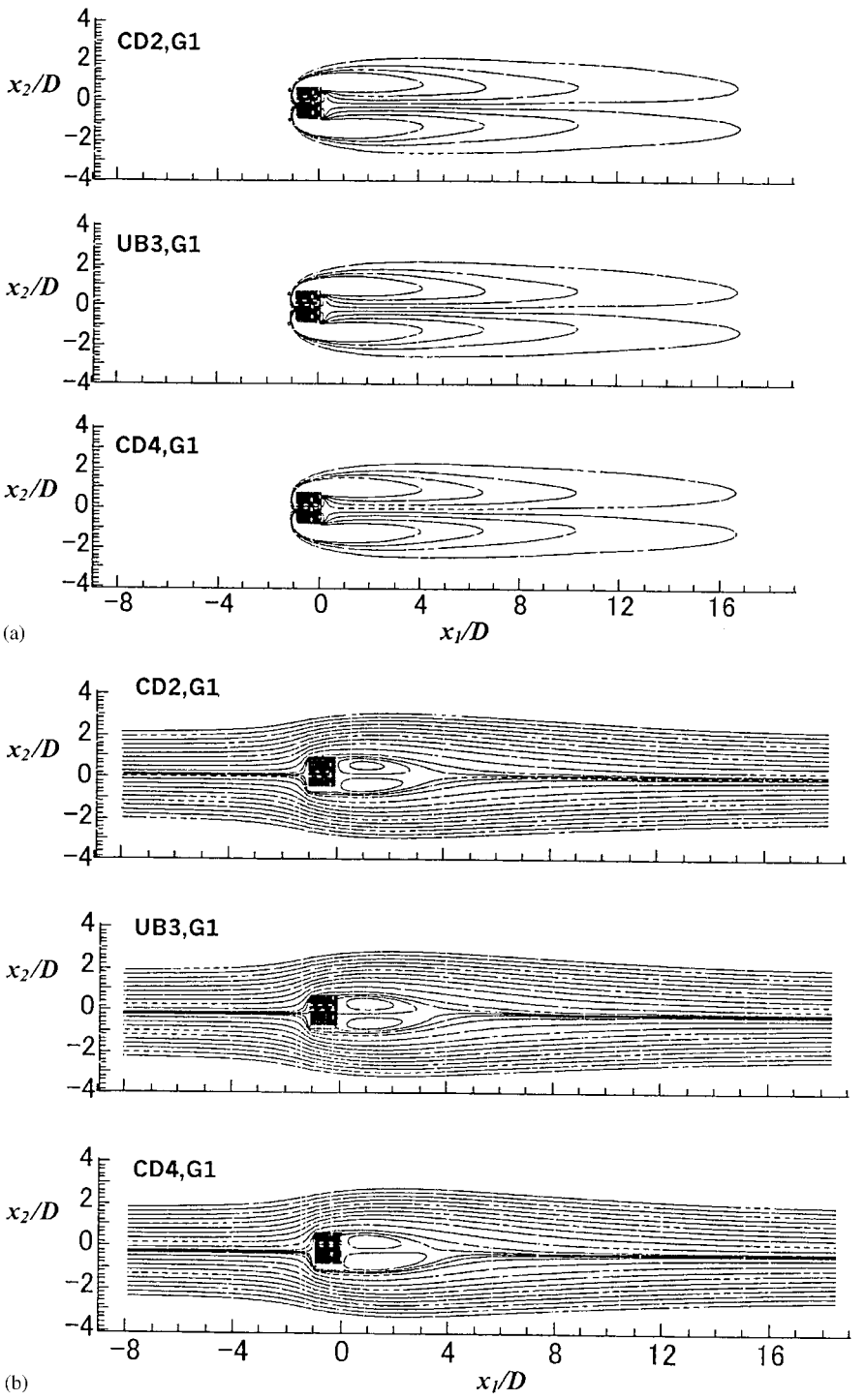

Figure 2. Calculation results for $Re = 50$: (a) contours of constant vorticity; (b) streamlines.

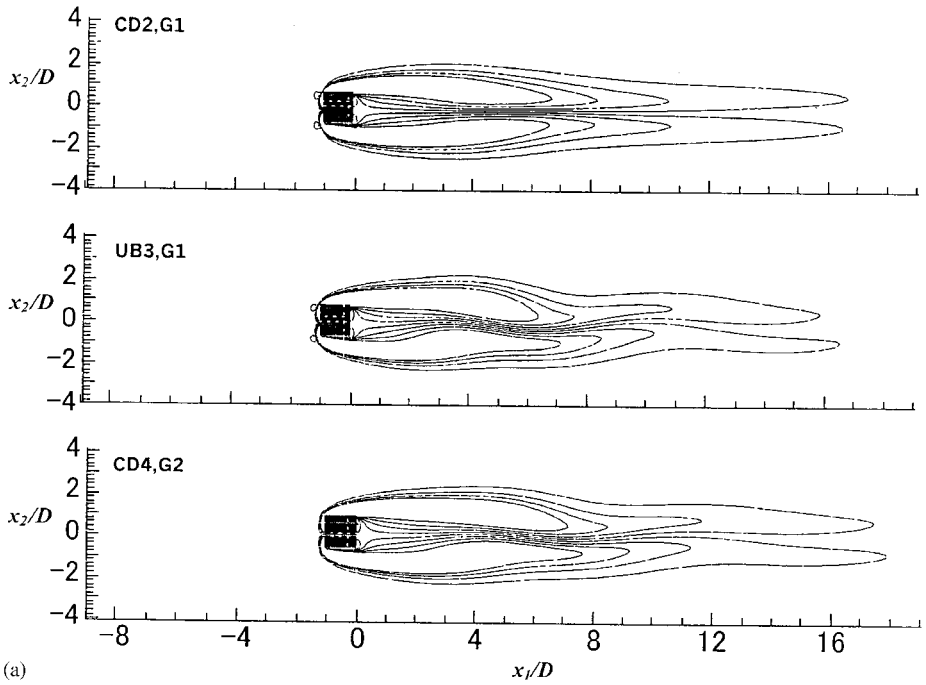

(a)

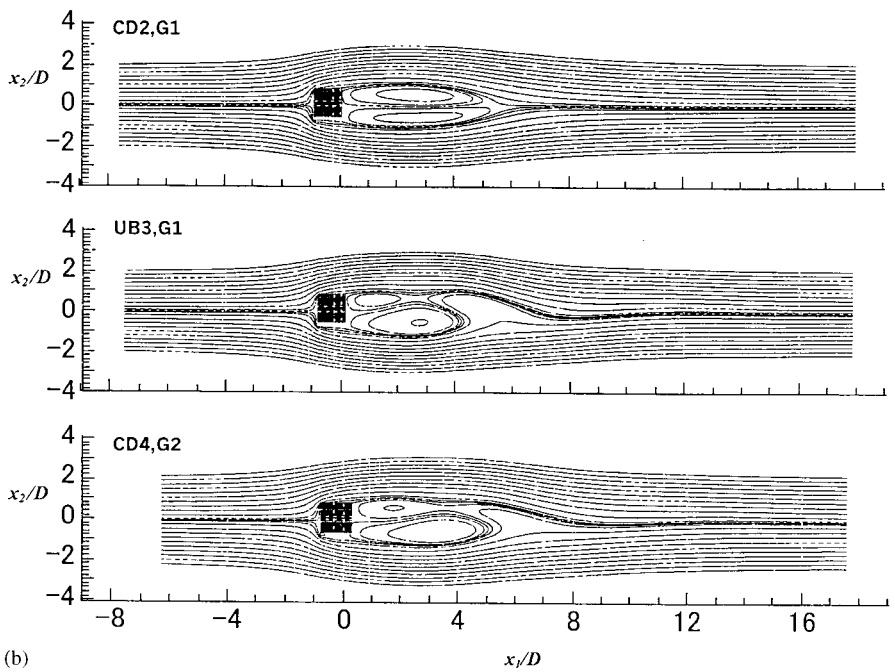

(b)

Figure 3. Calculation results for $Re = 100$: (a) contours of constant vorticity; (b) streamlines.

Table III. Calculated parameters for $Re = 100$.

Scheme and grid	Drag coefficient			Strouhal number
	Total	Due to pressure	Due to friction	
UB3, G2	1.626	1.565	0.061	0.162
CD4, G2	1.642	1.581	0.061	0.161
CD2, G1	1.522	1.465	0.057	0.152
Franke *et al.* [22]	1.61	1.55	0.06	0.165

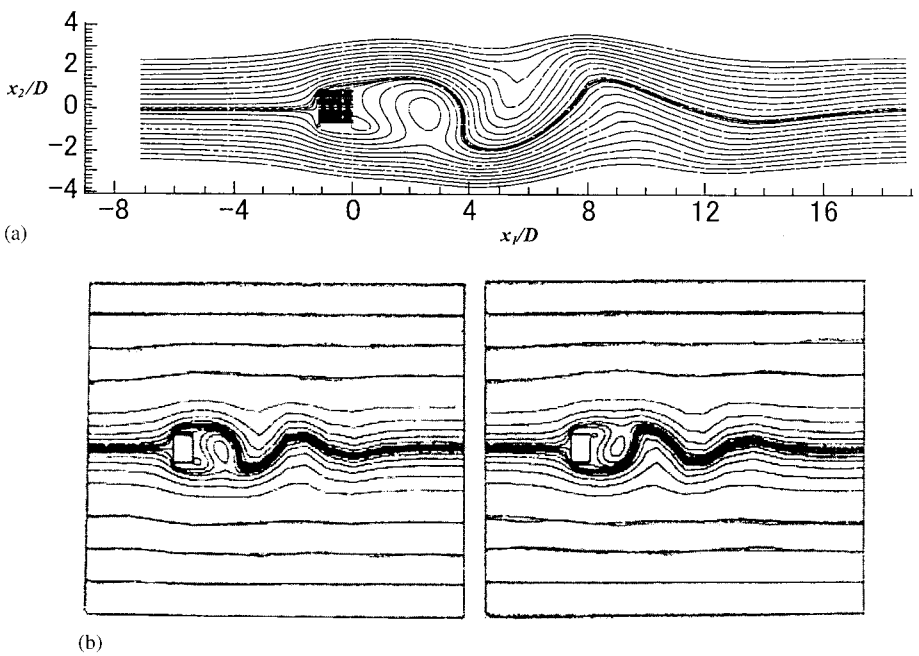

Figure 4. Calculation results for $Re = 150$ compared with Franke *et al.* [22] calculation: (a) present calculation with UB3 scheme and grid G1; (b) Franke *et al.* [22].

coarseness of the computational grid G1, only upwind-biased schemes survived the stability problems up to the Reynolds number of 500. Though the conservative CC2 scheme run on G2 did give results for $Re = 500$, it too started diverging at a higher Reynolds number. The central difference schemes, conservative or non-conservative, have dispersive errors and they all diverge at some Reynolds number below the laboratory Reynolds number for which we are interested in doing LES. This implies that for computation of turbulent flows at very high Reynolds numbers, the central differencing schemes have serious stability problems unless the grid has sufficient resolution and/or it is used with the subgrid-stress model that reduces the effective Reynolds number significantly and uniformly. The former remedy of using sufficient

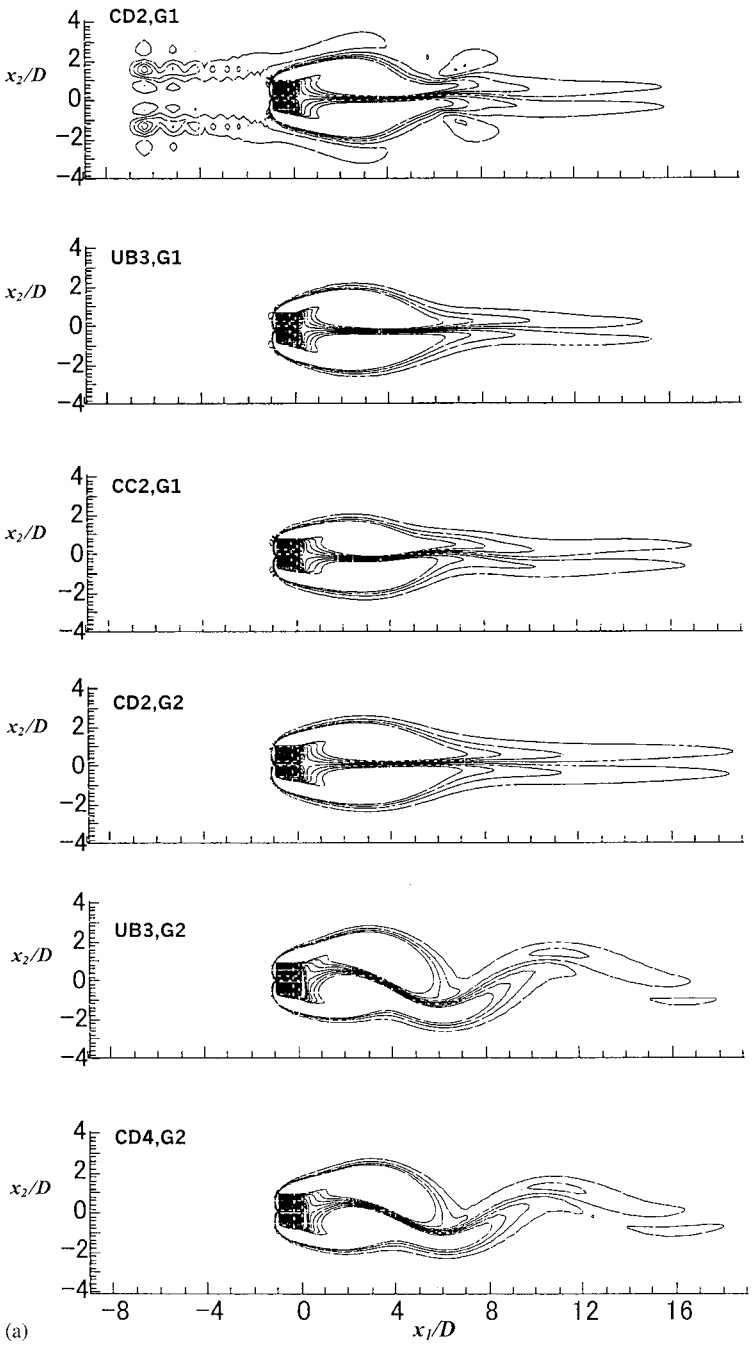

Figure 5. Calculation results for $Re = 200$: (a) contours of constant vorticity; (b) streamlines.

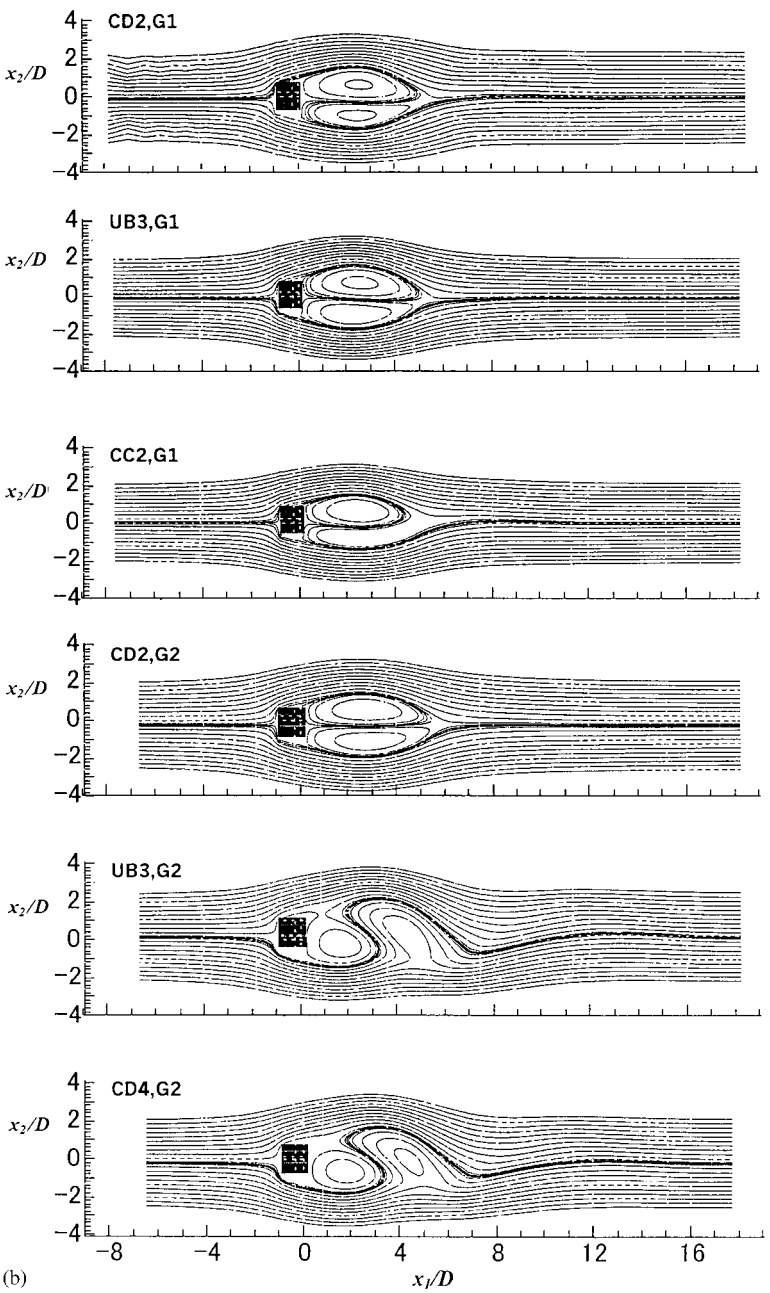

Figure 5. *Continued.*

grid resolution cannot and should not be hoped for in an LES. The dissipative errors that upwind-biased schemes suffer increasingly more with higher Reynolds number, may be or should be treated as part of the subgrid stress that just gives sufficient viscosity for stability.

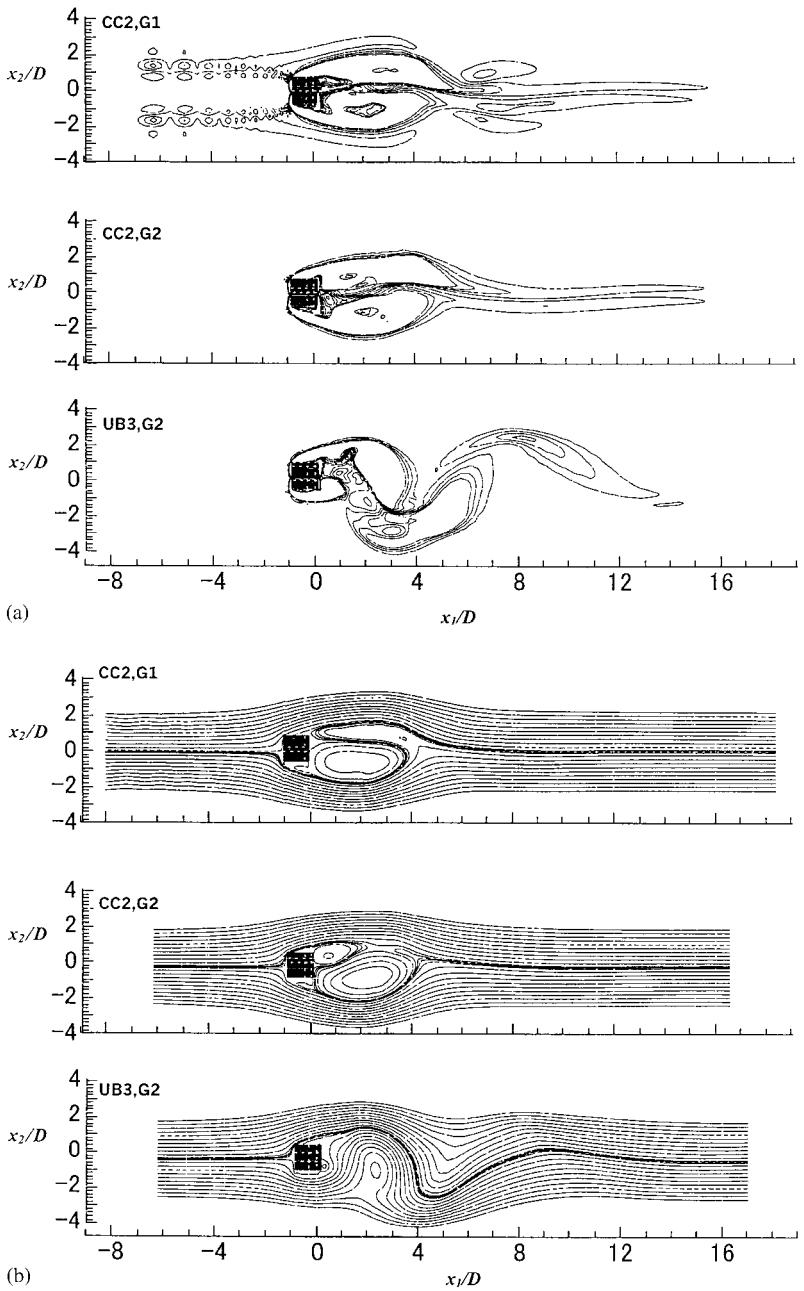

Figure 6. Calculation results for $Re = 500$: (a) contours of constant vorticity; (b) streamlines.

Then the subgrid turbulence stress model to be used will have to be that augments deficiency of this numerical viscosity. This conclusion somewhat contradicts the reported results of many simulations successfully performed with central difference schemes, but is what is arrived at

with the present method of fully implicit time advancing of the viscous terms and HSMAC procedure of pressure iteration. A recent work by Kogaki *et al.* [24] using a coarser grid, however, reports a similar conclusion as the present one.

5. CALCULATION OF TURBULENT FLOW AND COMPARISON WITH EXPERIMENTS

Here, we examine the turbulent flow calculation of Lyn's square cylinder test case [16, 17] at $Re = 22\,000$. Figure 7 shows instantaneous results, not necessarily at the same instance, of the contours of the constant spanwise vorticity calculated for this turbulent flow case with the standard Smagorinsky model with the difference schemes CC2, UB3 and UB5 on grid G2. Contrary to other reports of successful LES simulation using 2nd-order central difference schemes, the only central difference scheme that survived up to $Re = 500$, CC2, shows spurious oscillation problems at an early stage. The following calculations, therefore, are made only with the upwind-biased schemes UB3 and UB5. The turbulence models considered are the conventional Smagorinsky and dynamic Smagorinsky models as explained earlier. The results of the bulk parameters calculated by these methods are summarized in Table IV. These and the mean quantities shown below were obtained by averaging over eight vortex shedding cycles

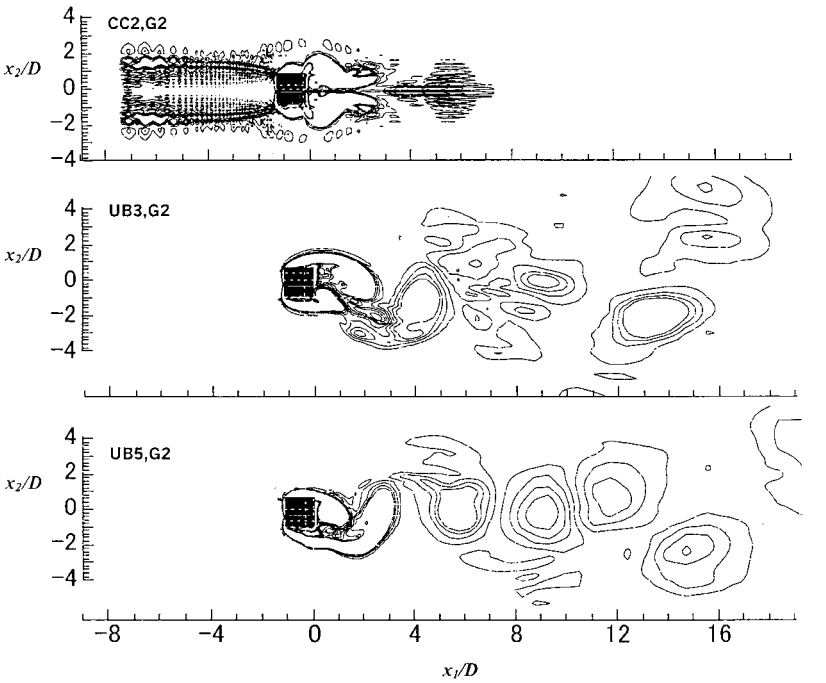

Figure 7. Calculation results for turbulent flow at $Re = 22\,000$ in terms of the contours of constant vorticity.

Table IV. Summary of calculated bulk parameters for turbulent case at $Re = 22\,000$.

Source	Scheme	Grid	SGS model	Mean drag coeff. (C_d)	RMS fluct. frag coef. ($C_{d,rms}$)	Max. back flow (U_m/U_{in})	Mean lift coef. (C_l)	RMS fluct. lift coef. ($C_{d,rms}$)	Length of recirc. region (L_R)	Strouhal no (St)
Lyn and Rodi [16]	Expt.	—	—	2.1		−0.215			1.38	0.132
Present	UB3	G1	Smag.	1.78	0.201	−0.229	−0.031	1.101	2.80	0.150
Present	UB3	G2	Smag.	2.20	0.127	−0.144	−0.023	1.236	1.28	0.135
Present	UB3	G2	Dynamic	2.24	0.118	−0.125	0.017	1.201	1.22	0.136
Present	UB3	G2	No model	1.88	0.121	−0.222	0.014	0.913	3.10	0.110
Present	UB5	G1	Smag.	2.02	0.251	−0.126	−0.011	1.151	1.32	0.125
Present	UB5	G2	Smag.	2.14	0.230	−0.139	−0.013	1.291	1.28	0.135
TAMU2 [5]	3rd-order upwind	$165 \times 113 \times 17$	Dynamic	2.77	0.190	−0.062	−0.09	1.79	0.94	0.14

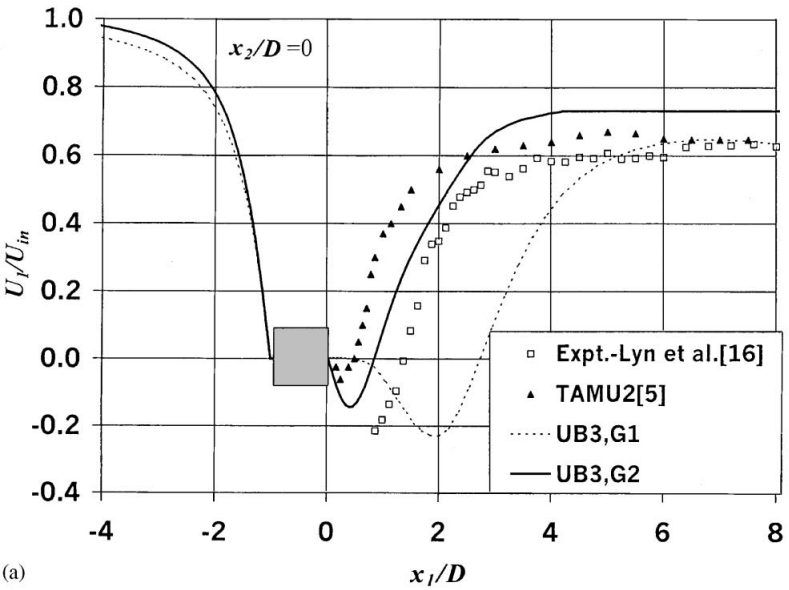

(a)

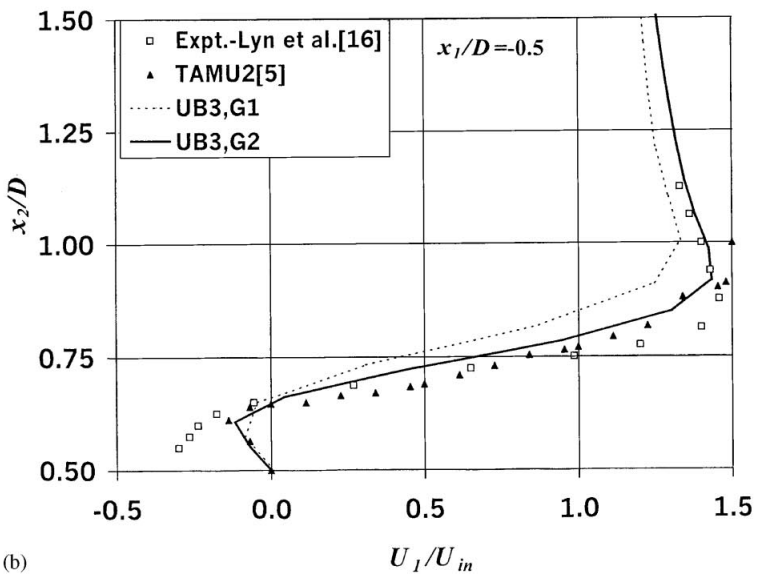

(b)

Figure 8. Calculation results of mean velocity in the wake and the boundary layer using different grids: (a) along the wake centerline; (b) in the boundary layer on the cylinder side, $x_1/D = -0.5$.

after an initial development time of $50D/U_{in}$. The mean lift coefficient over a sufficiently long time should be zero and its closeness to zero is an indication of accuracy of the time averaging. Experimental values of this quantity and the RMS fluctuations of the lift and drag coefficients are not available but listed here together with the calculation by Tamura, which

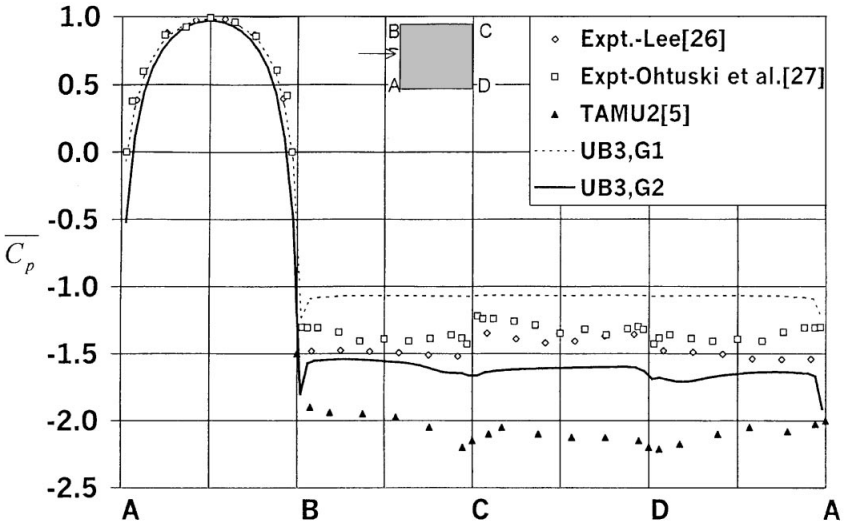

Figure 9. Calculation results of the surface pressure distribution using different grids.

is one of the best results reported at the workshop [5]. Although it is seen that the mean lift coefficient C_l is not quite zero but is sufficiently small compared with the RMS value for all calculation cases.

The details of the calculation results are presented by separately examining the effects of the grid resolution, order of accuracy of the difference schemes and the subgrid-stress models. A 3rd-order upwind scheme with the Smagorinsky model is taken as the reference and shown in each comparison together with experiments and one of the results of the workshop [5], so that ideas about their relation with other published calculations can be obtained.

5.1. Influence of grid resolution

On relatively easily accessible workstation-level computers, the total number of grid points that can be managed is around half a million points. Our choice of grid G1 is such that may be run on most computers very economically. It resolves the cylinder side into 20 sections but the boundary layer is not sufficiently resolved and the inner layer of the boundary layer even at the mid-point on the side surface is completely missed. Grid G2 uses about 50 per cent more points and resolves the boundary layer better but the first point from the surface still falls far outside the laminar sublayer of the boundary layer after reattachment. This implies that either grid is far from sufficient for resolving the small-scale motion next to the surface to be able to confidently apply the nonslip boundary condition. The instantaneous logarithmic law, which is often used in such cases, is even less sure to be applied in the present case with massive separation. This is a typical situation of practical LES of a complex flow at a large Reynolds number and how the small-scale motion near the wall is modeled or resolved may play a more important role than other aspects of the calculation and modeling. As Bouris and Bergeles [13] point out, capturing the near-wall motion may be more important than capturing

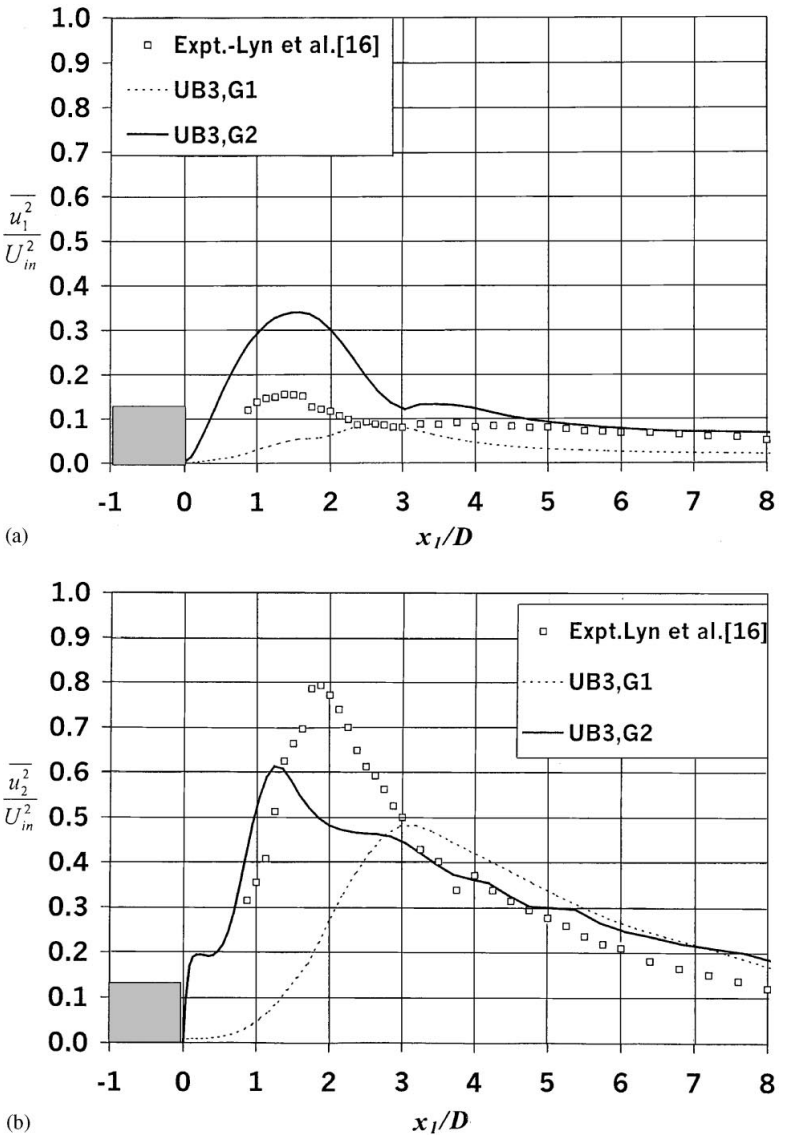

Figure 10. Calculation results of the fluctuation intensity using different grids: (a) streamwise fluctuation u_1^2/U_{in}^2 along the wake centerline; (b) transverse fluctuation u_2^2/U_{in}^2 along the wake centerline; (c) streamwise fluctuation u_1^2/U_{in}^2 in the boundary layer at $x_1/D = -0.5$.

the three-dimensional motion. We have tried this effective two-dimensional LES but we found that we could not take a sufficiently fine grid and the results did not come close to other methods and are not shown here. This point has been stressed by Spalart [25] who proposes a new method that uses a one-equation turbulence model to represent the small-scale boundary layer on the wall and a conventional LES in the separated flow region away from solid walls.

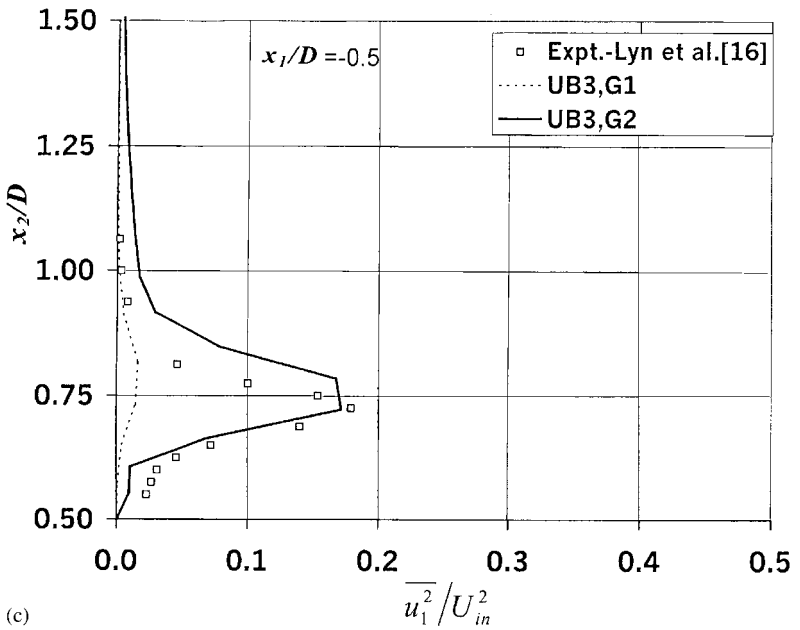

Figure 10. *Continued.*

Figure 8(a) and (b) show the distribution of the time-averaged streamwise velocity component, $U_1 = \overline{\langle u_1 \rangle}$ along the wake centerline and in the boundary layer at the center ($x_1/D = -0.5$) of the cylinder side surface, both compared with Lyn's experiment [16] and one of the best results, TAMU2, reported at the workshop [5]. It is seen that the results with grid G1 show far too long a recirculation region. Our results of UB3 on G2 with the conventional Smagorinsky model is seen to do about the same as TAMU2 [5] but the length of the recirculation region is closer to the experiment. Figure 9 shows a comparison of the results of the surface pressure compared with the experimental data of Lee [26] and Ohtsuki *et al.* [27]. The present results of UB3 on G2 are seen to be much closer to the experiment than Tamura's results. Figure 10(a), (b) and (c) compare the turbulent intensity components along the wake center line and in the boundary layer. Calculations with the coarse grid G1 appears just unacceptable in terms of turbulence as well, but the calculation using grid G2 gives reasonable results except that the streamwise intensity in the wake is overpredicted and the transverse intensity is underpredicted. What this means is that with the 3rd-order upwind-biased scheme and the conventional Smagorinsky model, the grid resolution at least as fine as the present G2 can give reasonable results, which may be better than those with the dynamic model.

5.2. *Order of accuracy of finite difference schemes*

Here we examine how the difference schemes of different orders of accuracy influence the results. For this purpose we show comparisons of the results with UB3 and UB5 schemes.

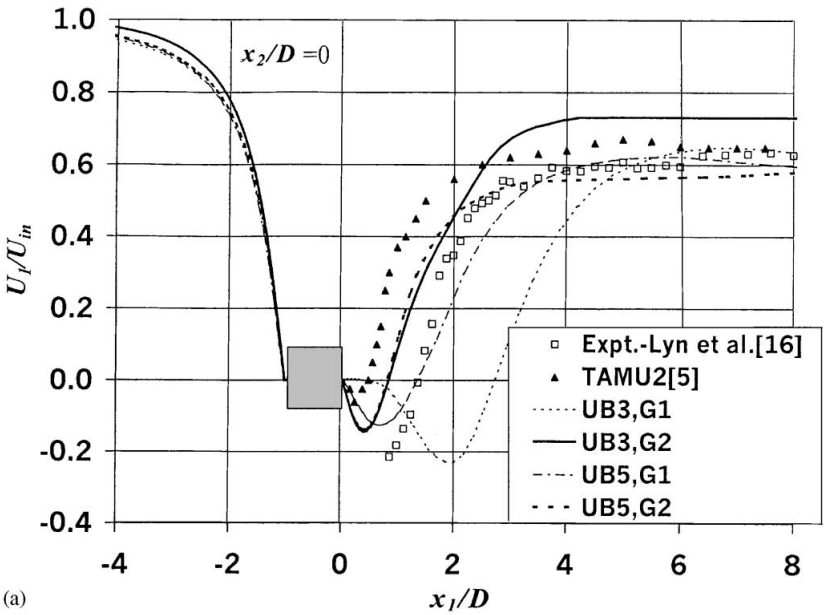

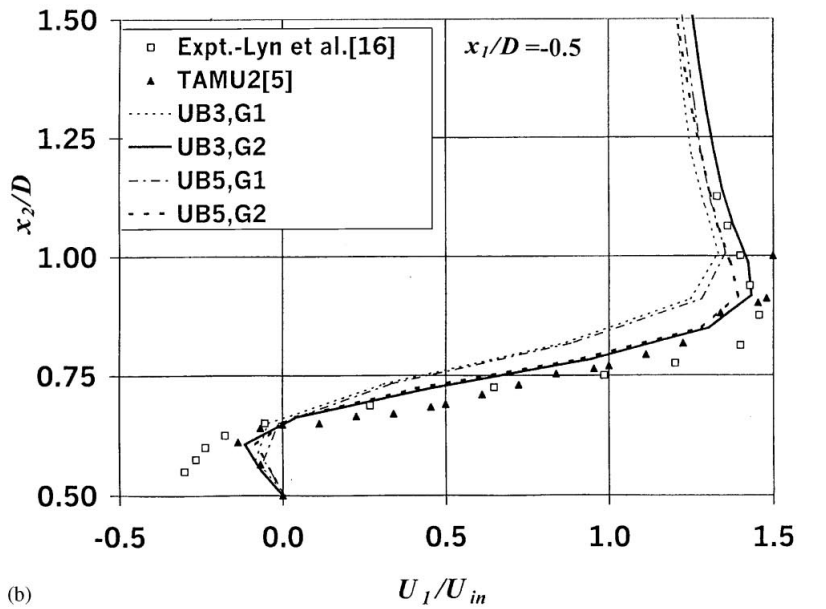

Figure 11. Calculation results of mean velocity in the wake and the boundary layer using different schemes and grids: (a) along the wake centerline; (b) in the boundary layer on the cylinder side, $x_1/D = -0.5$.

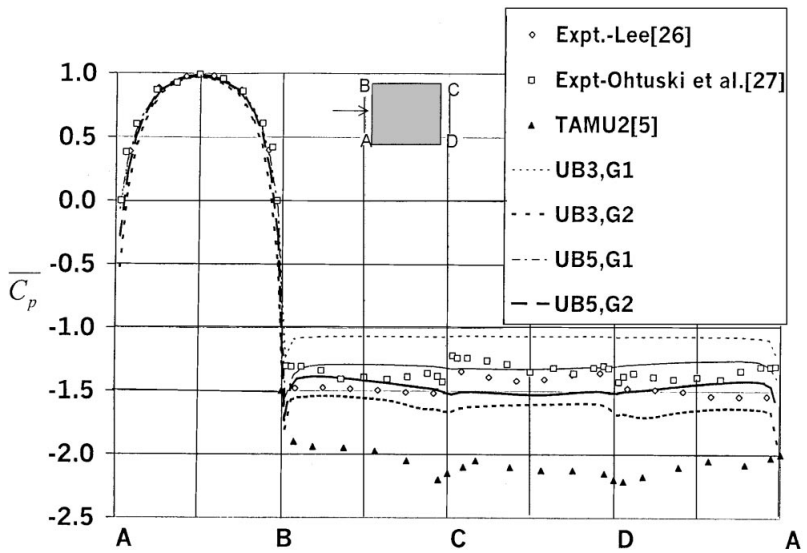

Figure 12. Calculation results of the surface pressure distribution using different schemes and grids.

Figure 11(a) and (b) shows the mean velocity along the wake centerline and the velocity profile in the boundary layer on the cylinder side just like Figure 8(a) and (b). It is seen that using the 5th-order scheme UB5 run on grid G2, the level of the mean velocity in the wake comes very close to the experiment, though the recirculation region is still much smaller than the experiment. The prediction of the surface pressure is shown in Figure 12. It also indicates that the higher order method on fine grid predicts the experiment very well. Figure 13 further shows the turbulence intensities in the wake and in the boundary layer. The overprediction of streamwise turbulence intensity $\overline{u_1^2}$, and underprediction of $\overline{u_2^2}$ seen in the results by UB3 are now significantly improved by using the higher order method UB5. The only exception may be that the transverse intensity in the near wake is seen to be slightly overpredicted, which perhaps is related to the underprediction of the recirculation region and its improvement will require better representation of the near-wall flow.

5.3. Influence of subgrid model

Here we examine if and how the results obtained with the standard Smagorinsky model may be altered by the dynamic subgrid model. Calculation results with the standard Smagorinsky model, the dynamic Smagorinsky model and without using a subgrid at all, all using the UB3 scheme on grid G2 are compared. The last case became unstable when run for a long time but did produce results up to the nondimensional time of about $100D/U_{in}$. Figures 14 through 16 are the same comparisons as done with Figures 8 through 10 for the grid resolution and Figures 11 through 13 for the order of difference schemes. The mean-velocity and the surface pressure

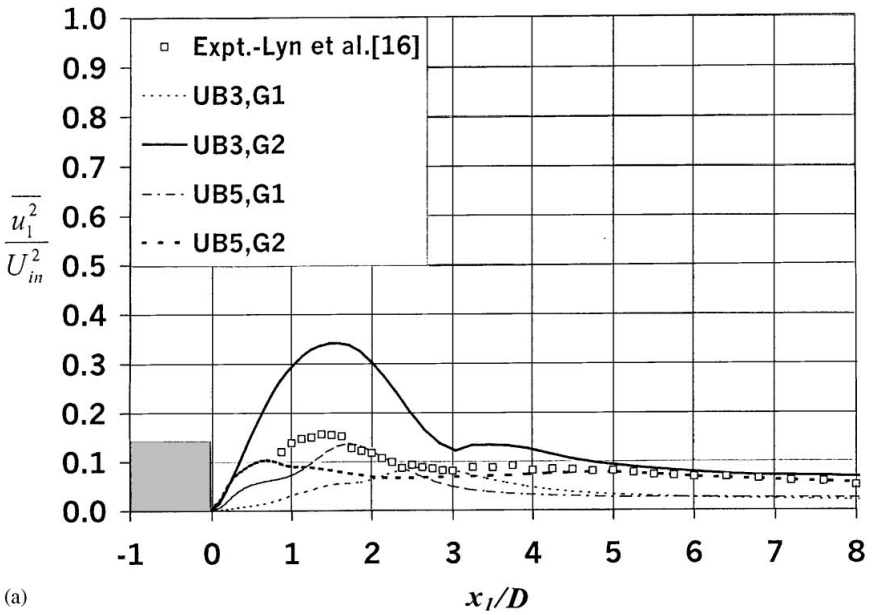

(a)

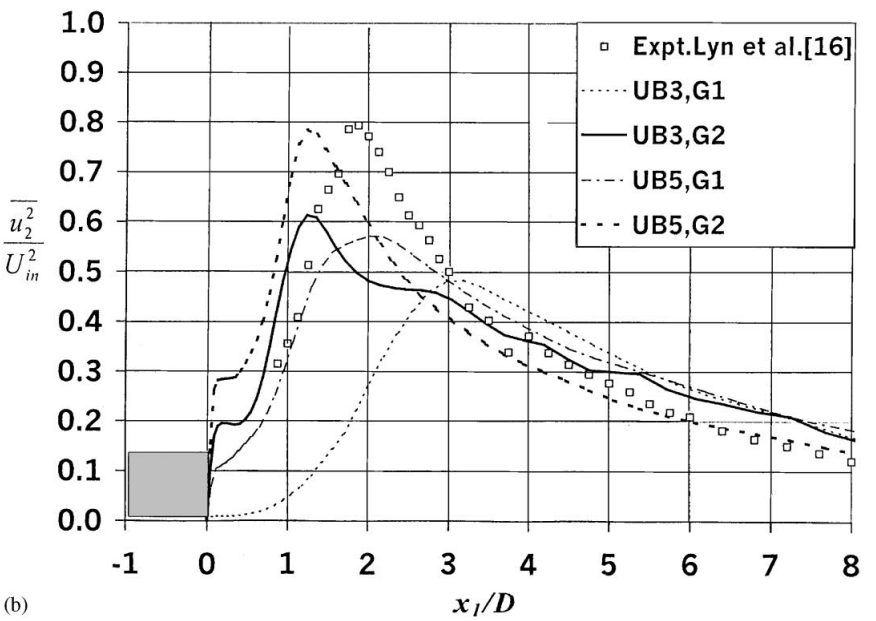

(b)

Figure 13. Calculation results of the fluctuation intensity along the wake centerline and the boundary layer using different schemes and grids: (a) streamwise fluctuation u_1^2/U_{in}^2 along the wake centerline; (b) transverse fluctuation u_2^2/U_{in}^2 along the wake centerline; (c) streamwise fluctuation u_1^2/U_{in}^2 in the boundary layer at $x_1/D = -0.5$.

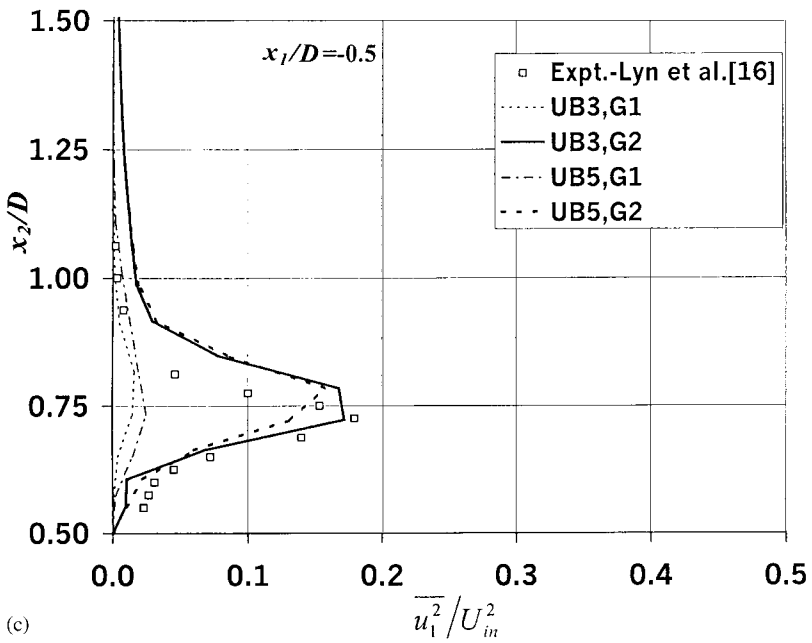

Figure 13. *Continued.*

results shown in Figures 14 and 15, show surprisingly similar improvements seen going from the UB3 scheme to UB5 scheme with the same Smagorinsky model. The turbulence results, shown in Figures 16(a) and (b), show somewhat different kinds of improvements than those obtained by the higher order differencing, but the magnitudes of improvements are very close. Hence, refining the subgrid model does nothing more than, but as much as, what the higher order scheme or the finer grids do.

The simulation without using any subgrid-stress model is seen to be way out of agreement with the experiment. This means that the numerical viscosity provided by the upwind-biased scheme may just be enough to conduct a stable calculation but nowhere enough to represent the physical subgrid turbulence viscosity.

5.4. Overall evaluation

The above results of various calculations and comparisons indicate that the better results of bluff-body turbulent-flow prediction at high Reynolds number can be obtained by any of the following methods of reducing the error in representing the subgrid stress. In other words, by increasing the grid resolution, increasingly smaller scale motion is resolved and the magnitude of the modeled part of turbulence reduces. By using the higher order difference scheme, the effective cut-off wave number is increased to reduce the subgrid stress again. By using a dynamic procedure, the local subgrid stress is represented more accurately. In carrying out these calculations, however, each of the refined methods required correspondingly larger

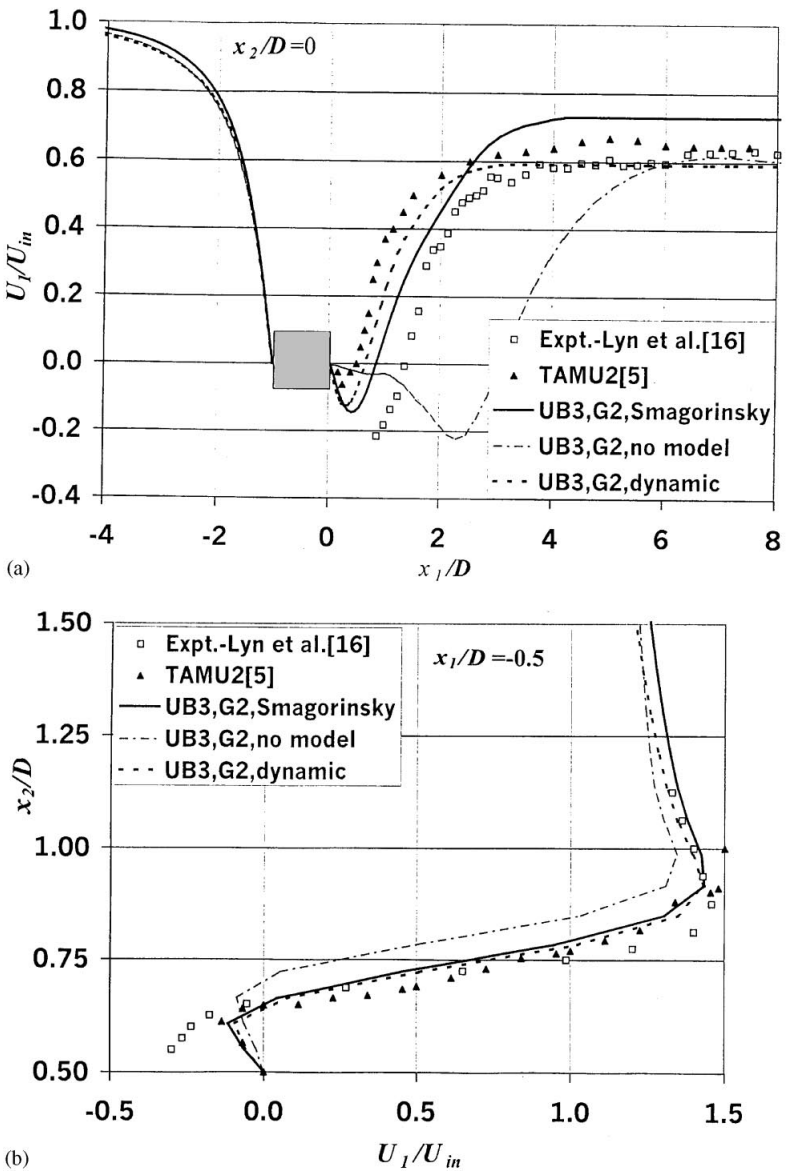

Figure 14. Calculation results of mean velocity in the wake and the boundary layer using different subgrid stress models: (a) along the wake centerline; (b) in the boundary layer on the cylinder side, $x_1/D = -0.5$.

amounts of computational time and storage space, and the method that has better merits will depend on different constraints dictated by the computational resources available in different situations.

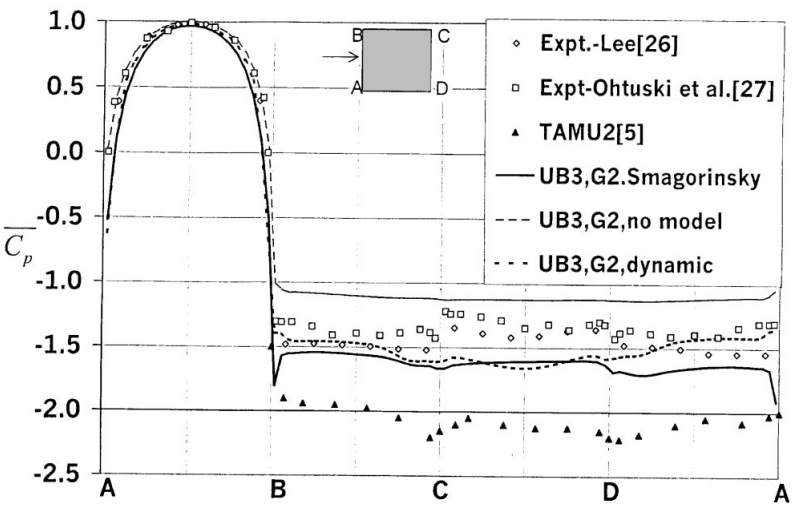

Figure 15. Calculation results of the surface pressure distribution using a different subgrid-stress model.

6. CONCLUSIONS

The following can be concluded from the results of the present computations of flow around a square cylinder using both central and upwind-biased finite-differencing schemes of various orders of accuracy, computational grids with different resolution, with conventional and dynamic eddy viscosity subgrid models, but with the same procedures of calculation in other aspects such as pressure iteration and time advancing methods.

With the total number of grid points kept within the limits of the capabilities of the workstation-level computers, the central differencing schemes of the realistic orders of truncation errors, the stability problems that appear upstream of the cylinder cannot be avoided for moderately high Reynolds numbers, and for turbulent flows used in conjunction with the eddy-viscosity model of the conventional or dynamic Smagorinsky types. This is distinct from the numerical schemes used in a DNS, in which the grid resolution is taken sufficiently fine to insure that all scales of motion are resolved. In LES calculations, the effects of the unresolved motion, which could have prevented instability, are not there and the physical turbulence model replacing them may not be enough to prevent instability. The upwind-biasing appears to provide just what is needed to prevent the calculation to diverge. The stabilizing effects of the numerical viscosity, however, do not replace the more versatile role of the subgrid stresses that need to be represented separately by a physical model such as the Smagorinsky model.

The 3rd-order upwind-biased scheme with conventional Smagorinsky model does fairly well if the grid used resolves the cylinder side into about 30 segments. Increasing the order of accuracy to the 5th-order or implementing the dynamic procedure improves the results of all pressure distribution, mean velocity distribution and turbulence stresses, but they all incur substantially increased computational loads, which may have been traded for a finer grid with better results for the lower order difference schemes.

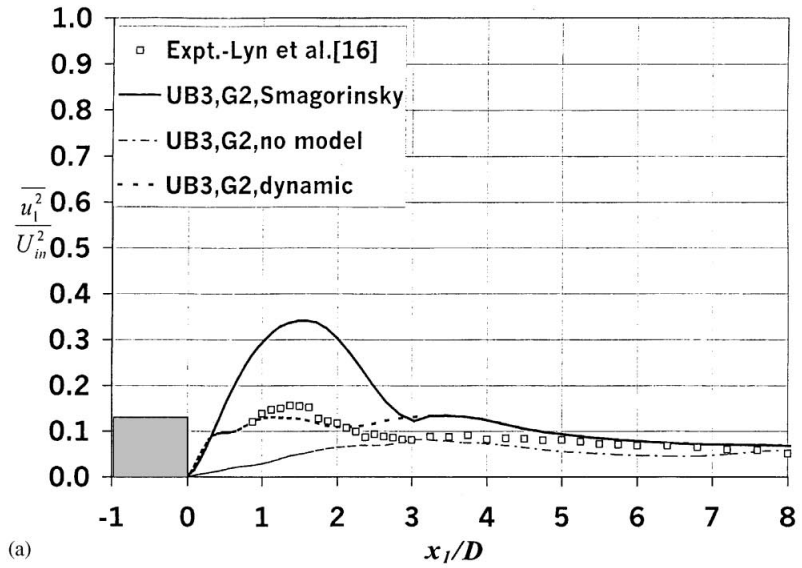

(a)

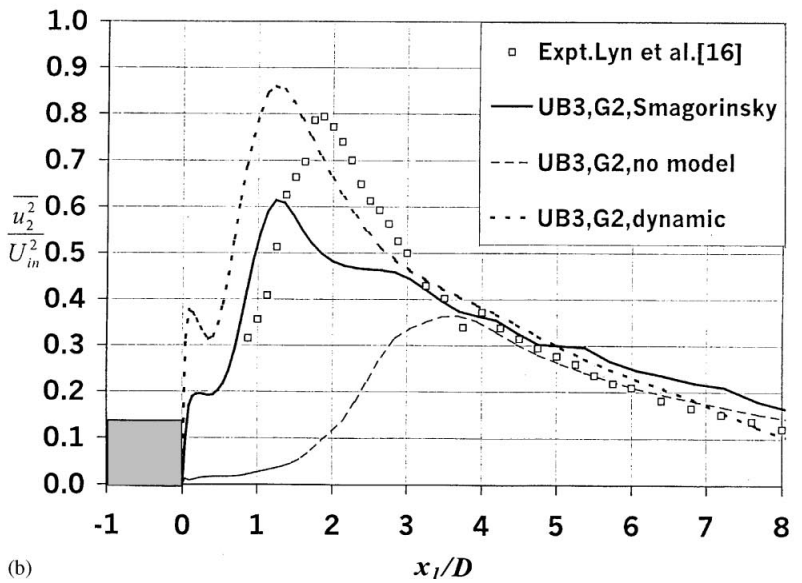

(b)

Figure 16. Calculation results of the fluctuation intensity along the wake centerline and the boundary layer using different subgrid stress-models: (a) streamwise fluctuation u_1^2/U_{in}^2 along the wake centerline; (b) transverse fluctuation u_2^2/U_{in}^2 along the wake centerline; (c) streamwise fluctuation u_1^2/U_{in}^2 in the boundary layer at $x_1/D = -0.5$.

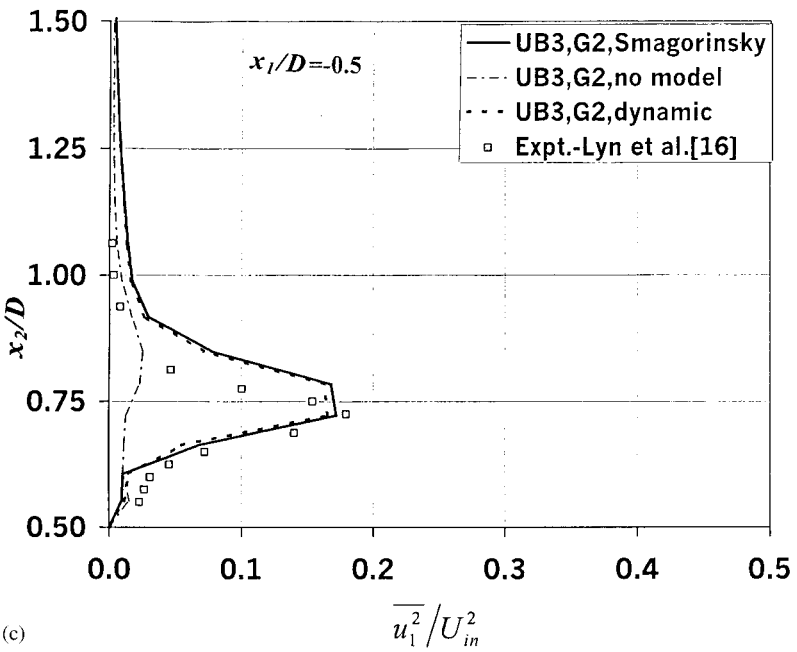

Figure 16. *Continued.*

Finally, resolving the near-wall low-Reynolds-number region at a cost of representing the spanwise direction, and hence the three-dimensionality, did not improve the overall accuracies. A prohibitively large grid is needed to capture the very small-scale accelerating flow around the sharp corner and the laminar sublayer of the separating boundary layers, which will be the key elements of further improvement such as better prediction of the length of the recirculation region, and an overwhelming enhancement of the quality of simulation may not be realized by further improving the order of accuracy or refining the subgrid-stress model.

REFERENCES

1. Johnson RW (ed.). Turbulence modeling and simulation. *Handbook of Fluid Dynamics*. CRC Press, Springer-Verlag, 1998.
2. Moin P. Numerical and physical issues in large eddy simulation of turbulent flows. *JSME International Journal Series B* 1998; **41**:454–463.
3. Murakami S. Overview of turbulence models applied in CWE—1997. *Journal of Wind Engineering and Industrial Aerodynamics* 1998; **74–76**:1–24.
4. Mason PJ. Large-eddy simulation: A critical review of the technique. *Quarterly Journal of Royal Meteorological Society* 1994; **120**:1–26.
5. Rodi W, Ferziger JH, Breuer M, Pourquie M. Status of large eddy simulation: Results of a workshop. *Journal of Fluids Engineering* 1997; **119**:248–262.
6. Morinishi S, Lund T, Vasilyev OV, Moin P. Fully conservative higher order finite difference schemes for incompressible flow. *Journal of Computational Physics* 1998; **143**:90–124.
7. Yoshizawa A, Horiuti K. A statistically-derived subgrid-scale kinetic energy model for the large-eddy simulation of turbulent flows. *Journal of Physics Society of Japan* 1985; **54**:2834–2839.
8. Germano M, Piomelli U, Moin P, Cabot WH. A dynamic subgrid scale eddy viscosity model. *Physics of Fluids A* 1991; **3**:1760–1765.

9. Bardina J, Ferziger JH, Reynolds WC. Improved subgrid-scale models for large eddy simulation. AIAA paper 1981–80, 1980.
10. Vreman B, Geurts B, Kuerten H. On the formulation of the dynamic mixed subgrid model. *Physics of Fluids A* 1994; **6**:4057–4059.
11. Fureby C, Tabor G, Weller HG, Gosman AD. Large-eddy simulation of the flow around a square prism. *AIAA Journal* 2000; **38**:442–452.
12. Sohankar A, Davidson L, Norberg C. Large eddy simulation of flow past a square cylinder: Comparison of different subgrid scale models. *Journal of Fluids Engineering* 2000; **122**:39–47.
13. Bouris D, Bergeles G. 2-D LES of vortex shedding from a square cylinder. *Journal of Wind Engineering and Industrial Aerodynamics* 1999; **80**:31–46.
14. Horiuti K. A new dynamic two-parameter mixed model for large-eddy simulation. *Physics of Fluids* 1997; **9**:3443–3464.
15. Najjar FM, Tafti DK. Study of discrete test filters and finite difference approximations for the dynamic subgrid-scale stress model. *Physics of Fluids* 1996; **8**:1076–1088.
16. Lyn DA, Rodi W. The flapping shear layer formed by flow separation from the forward corner of a square cylinder. *Journal of Fluid Mechanics* 1994; **267**:353–376.
17. Lyn DA, Einav S, Rodi W, Park JH. A laser Doppler velocimetry study of ensemble-averaged characteristics of the turbulent flow near wake of a square cylinder. *Journal of Fluid Mechanics* 1995; **304**:285–319.
18. Werner H, Wengle H. Large-eddy simulation of turbulent flow over and around a cube in a plate channel. *Proceedings of the 8th Symposium on Turbulent Shear Flows* 1991; 19.4.1–19.4.5.
19. Lilly DK. A proposed modification of the Germano subgrid-scale closure method. *Physics of Fluids A* 1992; **4**:633–635.
20. Fornberg B. Generation of finite difference formulas on arbitrary spaced grids. *Mathematics of Computation* 1988; **51**:699–706.
21. Nakayama A, Noda H. LES simulation of flow around a bluff body fitted with splitter plate. *Journal of Wind Engineering and Industrial Aerodynamics* 2000; **85**:85–96.
22. Franke R, Rodi W, Shoenung B. Numerical calculation of laminar vortex-shedding flow past cylinders. *Journal of Wind Engineering and Industrial Aerodynamics* 1990; **35**:237–257.
23. Sohankar A, Norberg C, Davidson L. Simulation of three-dimensional flow around a square cylinder at moderate Reynolds numbers. *Physics of Fluids* 1999; **11**:288–306.
24. Kogaki T, Kobayashi T, Taniguchi N. Large eddy simulation of flow around a rectangular cylinder. *Fluid Dynamics Research* 1997; **20**:11–24.
25. Spalart PR. Strategies for turbulence modelling and simulations. *Engineering Turbulence Modelling and Experiments* 1999; **4**:3–18.
26. Lee BE. The effects of turbulence on the surface field of a square prism. *Journal of Fluid Mechanics* 1975; **69**:263–282.
27. Ohtsuki H, Fujii K, Washizu H, Ohya A. On the characteristics of three components of aerodynamic forces and pressure distribution around a fixed rectangular cylinder in a uniform flow. *5th Symposium on Wind Loads on Structures* 1987; 169–175 (in Japanese).

